ELSEVIER

Earth and Planetary Science Letters 124 (1994) 19–33

EPSL

# The development of iron crust lateritic systems in Burkina Faso, West Africa examined with *in-situ*-produced cosmogenic nuclides

Erik Thorson Brown [a], Didier L. Bourlès [a], Fabrice Colin [b], Zakaria Sanfo [b], Grant M. Raisbeck [a], Françoise Yiou [a]

[a] *Centre de Spectrométrie Nucléaire et de Spectrométrie de Masse CNRS–$IN_2P_3$, Bâtiment 108, F-91405 Campus Orsay, France*
[b] *ORSTOM, UM GECO, Laboratoire de Géosciences de l'Environnement, Université Aix-Marseille III, F-13397 Marseille Cedex 13, France*

Received January 14, 1994; revision accepted April 15, 1994

**Abstract**

We have investigated the development of iron crust laterites on the stable West African Craton in northern Burkina Faso using cosmogenic radionuclides produced *in situ* in quartz veins and pebbles. Lateritic soils develop in tectonically stable, slowly eroding, tropical environments and are a major component of the Earth's surface. To examine processes affecting laterite formation, we determined $^{10}Be$ and $^{26}Al$ in samples of quartz from three sites representing two sequential and connected iron crust laterite systems. Results from outcropping quartz veins suggest that the mean erosion rate in this region is about 3–8 m $Myr^{-1}$. In addition, data from quartz cobbles and pebbles incorporated in iron crusts demonstrate that depth-dependent distributions of these nuclides may be used to distinguish surfaces undergoing burial from those undergoing erosive loss. Results from sections of the lowland lateritic system are consistent with mean accumulation rates of a few metres per million years. Quartz cobbles, presently at depths of a few metres in a paleochannel filled with rapidly deposited fluvial–colluvial material, have $^{10}Be$ distributions that suggest that the lowland lateritic surface may have formed during an erosive episode, presumably associated with a wetter climate, roughly 300 kyr BP. These results illustrate the practicality and the potential of the use of *in-situ*-produced cosmogenic nuclides for understanding the history of formation of laterites and for differentiating between systems formed through *in-situ* chemical weathering and mechanical transport.

## 1. Introduction

### *1.1. Formation of laterites: Chemical vs. physical processes*

Lateritic terrains cover over one third of the continents. Ecologically and pedologically sensitive environments, they are the substrate for equatorial forests and play a major role in local and global hydrological balances [1–3]. They have developed, essentially under tropical and subtropical climates, from long-term exposure of cratonic rocks to the atmosphere and hydrosphere. Bauxitic/ferralitic lateritic formations are present, with thicknesses up to 100 m, in what may be considered a transcontinental tropical belt of tectonically stable regions with low physical erosion rates.

[MK]


*SSDI* 0012-821X(94)00087-F

Most present-day laterites are polygenic, resulting from both physical and chemical transformations. These transformations, induced by changes in climate, occur laterally on the landscape scale and/or vertically on the scale of the relief of the initial weathered rocks. Understanding the formation of laterites requires consideration of *in-situ* biogeochemical and chemical weathering, and of transport of dissolved and supergene/residual (particles and pebbles) material, as functions of time. The issue of differentiating between *in-situ* and para-autochthonous/allochthonous processes has only recently been addressed [2,4] and poses challenges for future research.

The formation of successive aluminium/iron crust systems is believed to depend on climatic conditions: humid tropical for bauxites and humid tropical with contrasting seasons for iron crusts [5]. It has been proposed that the development of indurated iron crusts results from a progression of climatic conditions [3,5–7]. Iron crusts develop at depth in soil profiles during warm humid periods as iron is leached from the overlying soils and incorporated into secondary minerals at depth. This material is then indurated, becoming highly resistant to erosion, during ensuing dry periods. When such iron crusts are brought to the surface by erosion (probably associated with episodes of enhanced precipitation) they tend to persist as flat topographic highs as the surrounding landscape is degraded.

Direct dating of lateritic deposits and lateritization events has remained elusive. Relative ages can be obtained from geomorphological study of lateritic chronosequences as a function of climatic changes [8–10], from stratigraphic data on neighbouring sedimentary rock, and from dates on nearby volcanic rocks [11]. Paleoclimatic parameters can be investigated through oxygen isotope distributions in supergene phases such as kaolinite [12–15]. Recently, the $^{40}K$:$^{40}Ar$ and $^{40}Ar$:$^{39}Ar$ ages of K-rich manganese oxides in Brazilian laterites were used to quantify oxidation front progression during weathering [16]. Nevertheless, isotopic studies of supergene clay and oxide minerals are difficult because of fine particle sizes, and their interpretation is delicate because of the rapid and continual physical and chemical changes within lateritic systems.

Some constraints have been placed on the timing of development of laterite surfaces in West Africa. It has been proposed that high $CO_2$ levels, which are generally ascribed to intense volcanic activity, during the Siluro-Devonian and mid-Cretaceous–early Tertiary [17,18] resulted in warm and humid climates [19] that probably led to intensified weathering and development of bauxitic laterite formations. Assuming that the crust systems were formed by *in-situ* chemical processes, calculations based on differences in present-day mean elevations of the high-elevation bauxitic surface and the lowland iron crust lateritic system in Guinea, Mali and Senegal suggest that formation of these systems was initiated between 65 and 120 Myr BP and continued until approximately 1 Myr BP [3].

### *1.2. The use of in-situ-produced cosmogenic nuclides in examining exposure and burial processes*

It may be possible to distinguish between the *in-situ* chemical and allochthonous physical processes involved in laterite formation, to constrain physical denudation rates, and to date lateritization events through examination of distributions of cosmogenic nuclides produced *in situ* in exposed surficial rocks. Recent interest in these nuclides (which include $^{3}He$, $^{10}Be$, $^{14}C$, $^{21}Ne$, $^{26}Al$ and $^{36}Cl$) has focused primarily on their use in quantification of surface exposure ages. The following section will briefly outline the systematics of the production of cosmogenic nuclides in systems undergoing erosion and burial. A more detailed treatment of the temporal and spatial variability of cosmogenic nuclides in eroding and accumulating surfaces will be presented with the discussion of our results.

The rate of *in-situ* production of cosmogenic nuclides decreases exponentially with subsurface depth, and the production of these nuclides is limited to the upper few metres of Earth's crust. Therefore, as recently reviewed [20,21], exposure histories of surficial rocks are directly linked to the concentrations of these nuclides. In general, the concentration of a cosmogenic nuclide in rock

exposed at depth $x$ (g cm$^{-2}$) below a surface undergoing erosion at a rate of $\epsilon$ (g cm$^{-2}$ yr$^{-1}$) may be represented as a function of time $t$ (yr):

$$N(t, x) = \frac{P\, e^{-x/L}}{(\epsilon/L + \lambda)}[1 - e^{-t(\epsilon/L+\lambda)}] \quad (1)$$

where $P$ is the production rate (g$^{-1}$ yr$^{-1}$) at the altitude and latitude of the exposed surface, $L$ is the effective attenuation length of cosmic rays (values of $\sim 150$ g cm$^{-2}$ and $\sim 170$ g cm$^{-2}$ have been reported for solids at high and low latitudes, respectively [22–24]), and $\lambda$ is the radioactive decay constant (yr$^{-1}$). Depths are expressed in terms of overlying mass per unit area to eliminate dependence on rock and soil density. With the assumptions of negligible erosional loss and a single surface exposure episode, Eq. 1 may be used to calculate exposure ages.

In contrast, when surfaces are independently dated, cosmogenic nuclides may be used to constrain physical erosion rates. After a long period of exposure the concentration in the eroding surface approaches a steady-state value dependent only on the erosion rate. In this case ($t \to \infty$, $x = 0$) Eq. 1 may be rearranged to yield

$$\epsilon = L\left(\frac{P}{N(\infty)} - \lambda\right) \quad (2)$$

This relationship between steady-state concentrations of long-lived cosmogenic radionuclides and denudation rates can, in principle, constrain erosion rates varying from less than 1 m Myr$^{-1}$ to as much as 1000 m Myr$^{-1}$.

In an accumulating surface, the systematics of *in-situ* production differ from that in an eroding surface. If, because of environmental or climatic change, material from an exposed surface begins to be buried rather than eroded, the evolution of the cosmogenic nuclide concentrations takes a different form (comparable to that used by Lal et al. [25] to describe accumulation of *in-situ*-produced $^{14}$C in ice sheets):

$$N(t_B) = \frac{P\, e^{-t_B B/L}}{(-B/L + \lambda)}[1 - e^{-t_B(-B/L+\lambda)}] + N_0\, e^{-\lambda t_B} \quad (3)$$

In this equation, $B$ is a constant burial rate (g cm$^{-1}$ yr$^{-1}$), $t_B$ is the time since initiation of burial, and $N_0$ is the concentration at $t_B = 0$. In contrast to the models describing eroding surfaces, which examine rocks with reference to the surface (which at any given time represents a different piece of rock), this expression follows a given rock as it is deposited and buried. The present depth of that rock is equal to the product of the burial rate and the time since initiation of burial ($x = t_B B$). In an accumulating surface erosional loss no longer occurs, so cosmogenic nuclide concentrations can increase above the steady-state levels observed in regions undergoing erosion.

Additional information regarding exposure and burial of surficial rocks may be obtained from a ratio of cosmogenic radionuclides with differing halflives ($^{26}$Al:$^{10}$Be, with $t_{1/2}$ of 0.7 and 1.5 Myr, for example). Absolute concentrations are functions of both exposure time and subsurface depth, but ratios are essentially functions of only time, and their measurement may provide criteria for determining whether a sample has undergone extensive periods of burial [21,26].

Cosmogenic nuclides thus have the potential to act as tools for (1) estimates of exposure ages, (2) determination of physical denudation rates, (3) distinguishing surfaces undergoing erosion from those undergoing accumulation, and (4) quantification of burial rates of previously exposed material. Processes of exposure, erosion and burial play significant roles in the formation of laterites, so the distributions of cosmogenic nuclides in lateritic soil profiles should provide constraints on the timing and processes of their formation. To evaluate these methods we have determined $^{10}$Be and $^{26}$Al in a suite of quartz veins and cobbles associated with lateritic profiles from Burkina Faso, West Africa.

## 2. Site description

The investigated lateritic system has developed on the West African Craton in northern Burkina Faso at Belhouro (Fig. 1). Typical of most of the

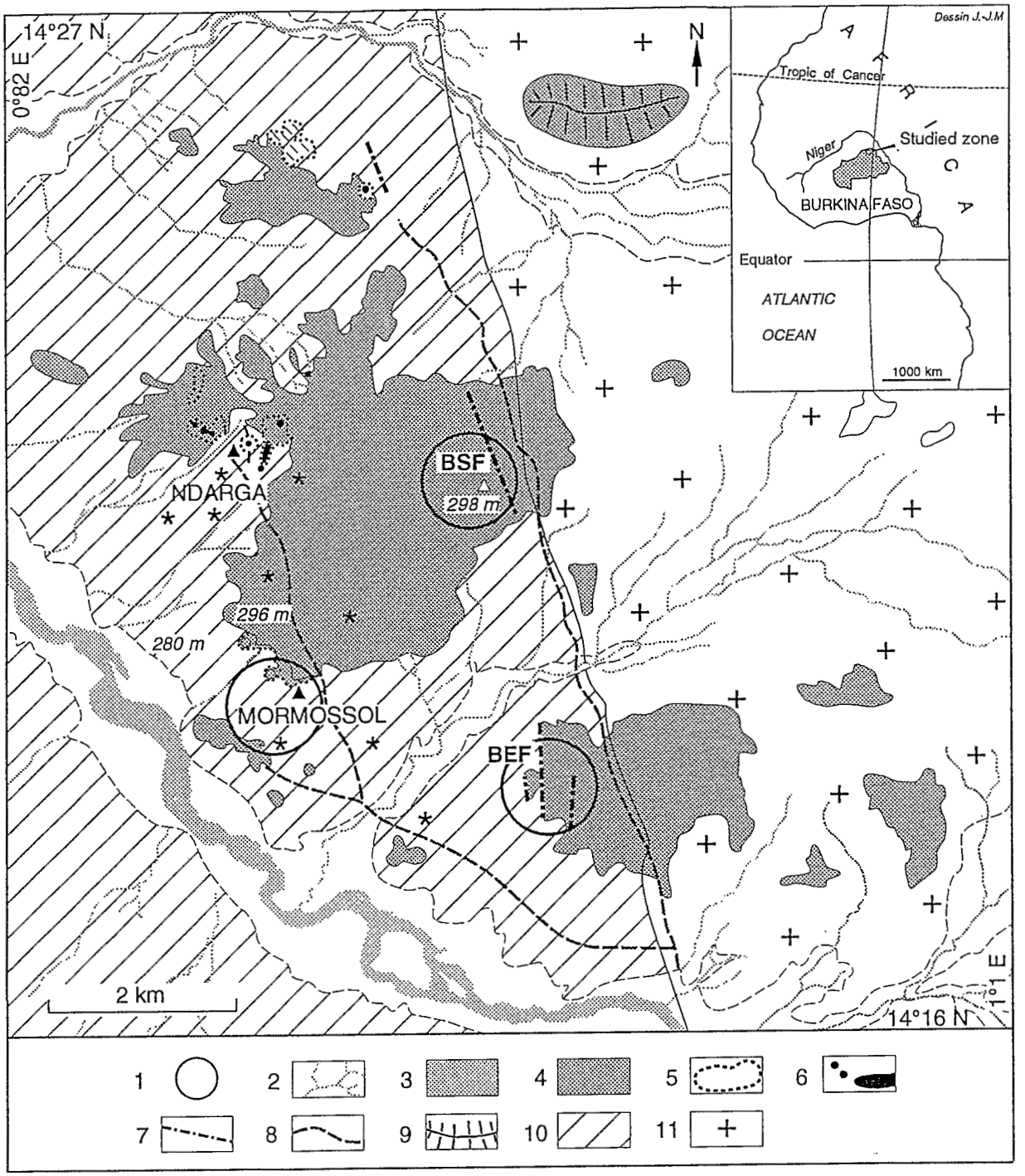


Fig. 1. Geomorphological and geological map of Belhouro. *1* = Sites included in this study; *2* = lowland lateritic system; *3* = regional river drainage; *4* = midland lateritic system; *5* = hills overlooking lowland and midland lateritic systems; *6* = highland lateritic system or older iron crust; *7* = quartz veins; *8* = roads; *9* = zones of high elevation with gentle slopes; *10* = upper Birrimian tuffaceous schist; *11* = lower Birrimian calc-alkaline granite; * = site of ancient gold exploitation; ▲ = site of present-day gold exploitation.

West African lateritic landscape [27,28], it is a complex iron crust system consisting of sequential surfaces that are laterally and geomorphologically connected. A series of stepped surfaces—the lowland, midland and highland lateritic systems —overlooked by elevated hills with gentle slopes has been defined throughout the region. It represents systems ranging in origin from present-day riverbeds to relicts of the African bauxitic peneplain (Fig. 1).

At Belhouro, the laterites have developed from weathering of Upper Birrimian tuffaceous schist and Lower Birrimian calc-alkaline granite. The present climate is Sahelo-Sudanese, with a mean annual rainfall of 55 cm. The vegetation is primarily Sahelian steppe with rolling forest, and occasionally grassy savanna, developing along river drainage axes. The iron crust system, which developed from schist with a NNW–SSE foliation, is crosscut by a roughly N–S oriented auriferous quartz vein field [29,30] (Fig. 1). These veins, which are a few metres thick and blue-grey and milky white in colour, have gold contents ranging from a few ppb to 50 ppm and potentially represent an economically viable deposit. Within the lowland, midland and highland laterites pebbles and cobbles of auriferous quartz have been found. These may be used to trace surface exposure history and to understand the genesis of these laterites.

## 3. Sampling and analyses

### 3.1. Sample collection

Three areas are included in the present study: BEF (Fig. 2a), BSF (Fig. 2b), and Mormossol (Fig. 2c). At Sites BEF and Mormossol, the quartz veins outcrop from the surface of the midland laterite system and define its border with the lowland system, in which quartz cobbles are scattered and buried. At BSF both the quartz veins and cobbles are present within the midland surface.

Material collected at Site BEF consists of three samples from outcropping quartz veins (two at the surface and one at depth) within the midland laterite and four large pebbles/small cobbles taken from the sandy clayey surface layer of the lowland lateritic system (Fig. 2a).

At Site BSF, an outcropping quartz vein was sampled at the surface and at depth and two samples, one from the sandy clayey layer and the other from the nodular layer, were taken from within the midland laterite (Fig. 2b).

At Mormossol one sample was taken at depth from a quartz vein located within the midland lateritic system, and in the lowland system three quartz pebbles were collected at various depths in a paleochannel cutting through the nodular layer and overlying the saprolite (Fig. 2c).

### 3.2. Analytical procedures

Crushed and sieved (500–1000 $\mu$m) quartz samples were prepared for analysis of cosmogenic nuclides. To eliminate the possibility of contamination by $^{10}$Be produced in the atmosphere, the samples were cleaned using sequential HF dissolutions [20]. After four HF steps, the cleaned quartz was completely dissolved in HF. The resulting solution was spiked with $^{9}$Be and (after determination of the natural level of $^{27}$Al by standard addition atomic absorption spectrophotometry) $^{27}$Al carriers. After separation of Be and Al by solvent extractions, BeO and $Al_2O_3$ were purified by extraction and precipitation [22,31]. All $^{10}$Be and $^{26}$Al measurements were performed by accelerator mass spectrometry at the Tandetron AMS Facility, Gif-sur-Yvette, France [32]. Analytical uncertainties (reported throughout as $1\sigma$) are based on counting statistics and conservative assumptions of 5% variability in machine response and a 30% uncertainty in the blank correction.

All calculations use production rates of 5.2 at $g^{-1}$ $yr^{-1}$ for $^{10}$Be and 31 at $g^{-1}$ $yr^{-1}$ for $^{26}$Al, based on the altitude- and latitude-dependent polynomials of Lal [21]. As discussed elsewhere [33], there may be uncertainties as large as 20% associated with these production rates. Such uncertainties have little effect on our conclusions.

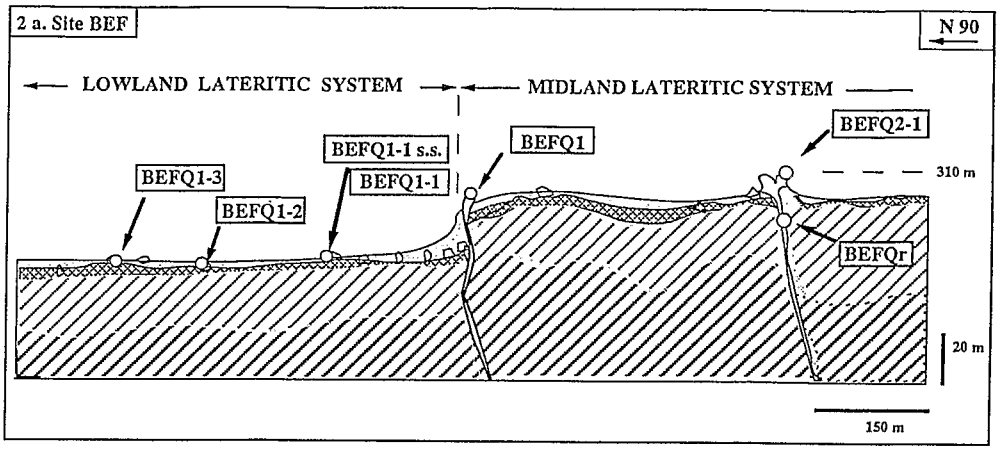
2 a. Site BEF
N 90
LOWLAND LATERITIC SYSTEM
MIDLAND LATERITIC SYSTEM
BEFQ1-3
BEFQ1-2
BEFQ1-1 s.s.
BEFQ1-1
BEFQ1
BEFQ2-1
310 m
BEFQr
20 m
150 m

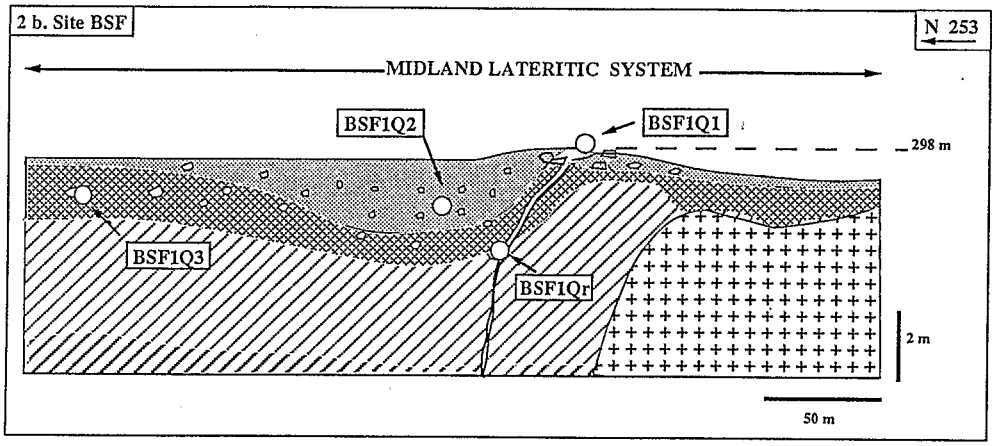
2 b. Site BSF
N 253
MIDLAND LATERITIC SYSTEM
BSF1Q2
BSF1Q1
298 m
BSF1Q3
BSF1Qr
2 m
50 m

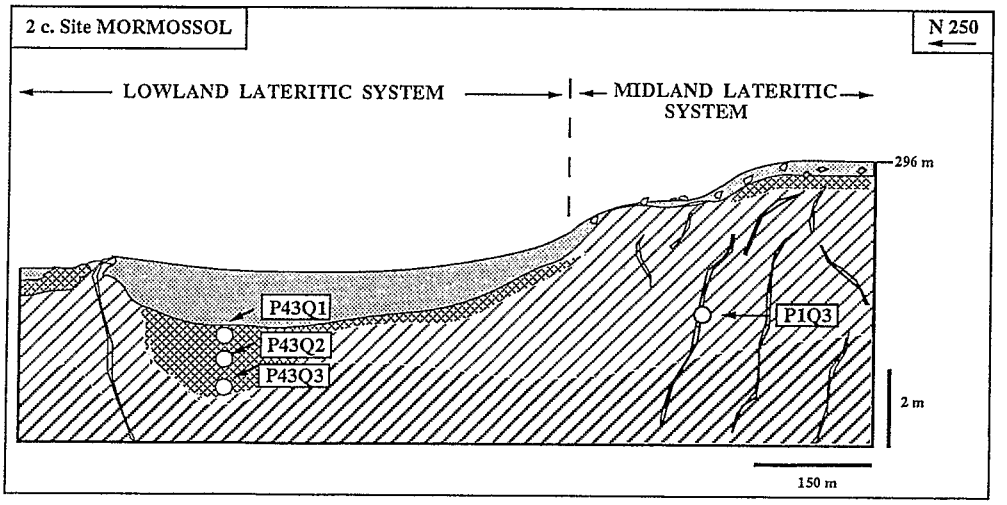
2 c. Site MORMOSSOL
N 250
LOWLAND LATERITIC SYSTEM
MIDLAND LATERITIC SYSTEM
296 m
P43Q1
P43Q2
P43Q3
P1Q3
2 m
150 m

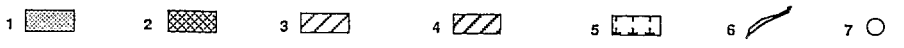
1
2
3
4
5
6
7

Table 1
Concentrations of *in-situ*-produced $^{10}Be$ and $^{26}Al$ in quartz from lateritic systems and calculated erosion rates

| sample ID | sample type | depth (g cm$^{-2}$) | sample mass (g) | $^{10}Be$ ($10^6$ at g$^{-1}$) | $^{26}Al$ ($10^6$ at g$^{-1}$) | $^{26}Al$:$^{10}Be$ (at at$^{-1}$) | erosion rate* (m Myr$^{-1}$) |
|---|---|---|---|---|---|---|---|
| BSF1-Q1 | vein quartz | 0 | 4.80 | 1.03±0.09 | 5.27±1.17 | 5.10±1.22 | 2.9 |
| BSF1-Q2 | quartz cobble | 89 | 10.53 | 1.84±0.13 | 9.95±1.32 | 5.42±0.81 | |
| BSF1-Q3 | quartz cobble | 237 | 9.17 | 1.73±0.12 | 10.00±0.97 | 5.79±0.70 | |
| BSF1-Qr | vein quartz | 530 | 6.18 | 0.38±0.05 | 1.54±0.50 | 4.08±1.41 | |
| P1Q3 | vein quartz | 373 | 5.90 | 0.070±0.029 | 0.27±0.24 | 3.95±3.86 | 4.4 |
| P4-3Q1 | quartz cobble | 403 | 7.43 | 0.53±0.06 | 4.06±0.59 | 7.71±1.43 | |
| P4-3Q2 | quartz cobble | 563 | 5.49 | 0.27±0.04 | 0.97±0.46 | 3.52±1.74 | |
| P4-3Q3 | quartz cobble | 725 | 8.20 | 0.095±0.021 | 1.10±0.43 | 11.51±5.14 | |
| BEFQ1 | vein quartz | 0 | 16.78 | 0.39±0.03 | 3.05±0.45 | 7.74±1.27 | 8.1 |
| BEFQ2-1 | vein quartz | 0 | 9.07 | 0.61±0.04 | 3.73±0.38 | 6.08±0.76 | 5.1 |
| BEFQr | vein quartz | 398 | 16.05 | 0.046±0.007 | 0.67±0.17 | 14.50±4.17 | 5.7 |
| BEFQ1-1 | quartz cobble | 0 | 17.09 | 1.48±0.08 | 9.33±0.64 | 6.29±0.56 | |
| BEFQ1-1s.s. | friable quartz cobble | 0 | 19.23 | 1.65±0.10 | 8.54±0.50 | 5.17±0.43 | |
| BEFQ1-2 | quartz cobble | 0 | 16.67 | 1.68±0.22 | 10.55±0.52 | 6.28±0.87 | |
| BEFQ1-3 | quartz cobble | 0 | 13.54 | 0.75±0.05 | 4.37±0.34 | 5.86±0.61 | |

[a] Rates calculated from $^{10}Be$ concentrations in samples from outcropping quartz veins. The measured concentrations for samples collected at depth were normalized to surface values using an attenuation length of 170 g cm$^{-2}$.

## 4. Results

Measured $^{10}Be$ concentrations range from 300 to $1800 \cdot 10^3$ at g$^{-1}$ (Table 1) and may be divided into two general groups, those from iron crust surfaces (the lowland and part of the midland laterites) and those from quartz veins (part of the midland laterites). Although the quartz vein samples are from older, higher elevation surfaces, they nearly systematically have lower $^{10}Be$ concentrations than those from the lower surfaces. While at first this appears counterintuitive—one would expect the older surfaces to have higher $^{10}Be$ levels—it is consistent with a scenario in which the material undergoing burial in the lower surfaces had been exposed in source regions in the upper surfaces before transport to its present positions.

The $^{26}Al$ results, with concentrations ranging from 2000 to $10{,}000 \cdot 10^3$ at g$^{-1}$ (Table 1), are generally coherent with those of $^{10}Be$. Because of relatively high levels of natural $^{27}Al$, the measured $^{26}Al$:$^{27}Al$ ratios were extremely low in some samples, resulting in large analytical uncertainties. Ratios of $^{26}Al$:$^{10}Be$ for most samples fall in a range consistent with the production ratio of $6.04 \pm 0.44$ [34] and with erosion rates greater than $\sim 10$ m Myr$^{-1}$ (see [21] for a discussion of $^{26}Al$:$^{10}Be$ evolution as a function of exposure time). However, two samples collected from substantial subsurface depth have somewhat higher values of $^{26}Al$:$^{10}Be$.

Anomalously high $^{26}Al$:$^{10}Be$ ratios have been reported in other rocks with relatively low cosmogenic nuclide concentrations. It has been proposed that this may be a result of nucleogenic

Fig. 2. Schematic cross sections showing distributions of layers within weathering mantles and sample locations for Sites BEF (a), BSF (b) and Mormossol (c). *1* = Surface layer (sandy–clayey or sandy–gravelly); *2* = nodular layer (locally indurated iron crust with diffuse iron nodules; *3* = saprolitic layer (kaolinitic and/or smectitic with recognizable schist textures; *4* = unaltered schist; *5* = calc-alkaline granite; *6* = quartz veins; *7* = quartz samples (note that at the Mormossol site the pit samples were taken from a paleochannel cutting into the saprolite).

reactions induced by radioactive decay of uranium and thorium and their daughter products [20,35]. Both $^{10}$Be and $^{26}$Al can be produced through the alpha-capture reactions $^{7}$Li($\alpha$,$p$)$^{10}$Be and $^{23}$Na($\alpha$,$n$)$^{26}$Al, and $^{10}$Be can result from the reactions $^{9}$Be($n$,$\gamma$)$^{10}$Be, $^{10}$B($n$,$p$)$^{10}$Be and $^{13}$C($n$,$\alpha$)$^{10}$Be in which the neutrons are induced by ($\alpha$,$n$) reactions. Measurements of $^{10}$Be and $^{26}$Al in various uranium and thorium ores indicate that production rates of $^{10}$Be are vanishingly small (because of the low concentrations of target nuclei) but that significant quantities of $^{26}$Al may result from these reactions [36]. Assuming uniform distributions of elements, Sharma and Middleton [36] calculated that $60 \cdot 10^3$ at g$^{-1}$ of $^{26}$Al would be supported by radiogenic production in average quartz sandstone. However, because these reactions are spatially limited by the alpha-recoil distance in quartz, production of $^{26}$Al is likely to be dependent on the microscopic distributions of U and Th relative to Na, the major target element. In samples such as ours, these elements are likely to be concentrated in accessory minerals, inclusions, and iron oxide coatings. We are initiating a quantitative study of this phenomenon.

The concentrations of $^{26}$Al in the samples with anomalous ratios are among the lowest in the dataset. Comparison of $^{10}$Be and $^{26}$Al results for these samples indicates that the concentration of $^{26}$Al in excess of that produced by cosmic ray neutron induced spallation is less than $400 \cdot 10^3$ at g$^{-1}$, suggesting that the contribution of nucleogenic $^{26}$Al is minor in the other samples.

## 5. Discussion

### 5.1. Eroding surfaces

Interpretation of the results from the outcropping quartz veins (from parts of the midland lateritic surface) is relatively straightforward. If the exposure ages of these surfaces are sufficiently long for $^{10}$Be and $^{26}$Al to have reached a steady-state balance between production and loss due to radioactive decay and to erosion, the concentrations of these nuclides may be used to estimate physical denudation rates (see Eq. 2). Based on geomorphological and petrological studies of similar lateritic systems in the Ivory Coast, Delvigne and Grandin [9] and Boulangé et al. [10] concluded that the African bauxitic surface was formed during the humid period of the upper Cretaceous to Eocene. Further calculations based on comparison of present-day elevations of relicts of the bauxitic surface with those of lower indurated iron crusts suggest that the African bauxites developed between 65 and 120 Myr B.P. and that the midland lateritic system began to form about 5 Myr ago [3]. Although these chronologies are based on qualitative studies, the resulting ages justify our steady-state assumption.

Samples of outcropping quartz veins (either from the surface or from depth, corrected to surface concentrations assuming an attenuation length of 170 g cm$^{-2}$) yield erosion rates ranging from 3 to 8 m Myr$^{-1}$ (Table 1). These imply very slow denudation, consistent with the relative tectonic quiescence of the West African Craton. These values are comparable to a rate of 8.3 m Myr$^{-1}$ estimated from watershed mass balance of the Lake Chad drainage basin [37]. Our results are also consistent with values ranging from 6 to 12 m Myr$^{-1}$ calculated from the relative elevations on the regional scale of these lateritic systems [3]. Similarly low rates of physical erosion have been reported for other cratons. Brown et al. [38] reported a rate of $\sim$1 m Myr$^{-1}$ for the summit of Mount Roraima, Venezuela, a site which has been interpreted as a relict of the Gondwanaland Surface [39]. Rates of 1–2 m Myr$^{-1}$ have been suggested for the Yilgarn Block in southwestern Australia [40,41] and for other Australian bedrock surfaces [42,43].

### 5.2. Accumulating surfaces

In contrast, the iron crust surfaces (parts of the midland surface and the lowland surface) show evidence of active accumulation. The following section will describe how the distribution of $^{10}$Be in surface deposits (BEF) and profiles (Mormosol and BSF) in such regions can yield constraints on the history of their formation. In

addition, it will describe the added information obtained in these systems through examination of $^{26}Al:^{10}Be$ ratios.

*Recent deposition on accumulating surfaces*

Site BEF encompasses both the midland and lowland lateritic systems (Fig. 2a). As described above, the samples of the outcropping quartz veins in the midland system are believed to have steady-state $^{10}Be$ concentrations with respect to physical erosional loss. Field evidence (similar coloration of quartz at both locations and the general scarcity of vein quartz in the region) indicates that such outcrops are likely to be the source rock for the lowland samples. Samples from the lowland laterite have $^{10}Be$ concentrations that are nearly consistently higher than those from the assumed source region, in accordance with the assumption that erosional loss does not affect material undergoing slow burial. Fig. 3 shows a model of the accumulation of $^{10}Be$ as a function of time in a bedrock surface eroding at 5 m $Myr^{-1}$ and in cobbles (which had the steady-state concentration of the eroding surface as their initial concentration) undergoing burial at rates of 2, 4 and 6 m $Myr^{-1}$. The cosmogenic nuclide concentrations of rock undergoing slow burial exceed the steady-state concentration in the eroding source rock. Measured $^{10}Be$ concentrations from outcropping quartz veins and from quartz pebbles incorporated within the lateritic soils are plotted—with arbitrary positions on the time axis—over the model curves. The results from from the outcropping veins are consistent with steady-state erosion rates of several metres per million years (Table 1). Data from the lateritic soils suggest that burial may be occurring at a comparable rate (Fig. 3). Assuming that the $^{10}Be$ measured in the midland system quartz veins is representative of the concentrations of the lowland samples at the time of their deposition, the difference in concentration between the lowland and midland samples (up to $\sim 10^6$ at $g^{-1}$) suggests that the lowland system has been active for at least several hundred thousand years.

*Earlier deposition on accumulating surfaces*

Because samples from Site BSF (within the midland laterite system, Fig. 2b) are presently at substantial depth, it is necessary to consider the systematics of cosmogenic nuclide accumulation as a function of depth in surfaces undergoing

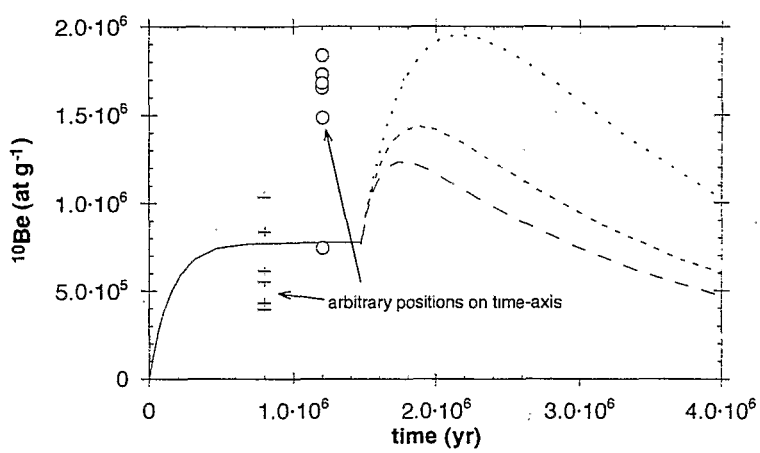


Fig. 3. Model of $^{10}Be$ as a function of time in rock undergoing erosion followed by burial: comparison with data from quartz veins and lateritic surfaces. The calculations are based on a rock eroding at a rate of 5 m $Myr^{-1}$ (continuous line), reaching steady-state concentration, and being deposited onto and buried at rates of 2 (short dashes), 4 (medium dashes) and 6 (long dashes) m $Myr^{-1}$ in an accumulating surface. Data from outcropping quartz veins (+) and from lateritic surfaces (○) are overlain on the model curves, with arbitrary positions on the horizontal axis. The samples from eroding veins (subsurface samples have values normalized to the surface assuming an exponential attenuation length of 170 g $cm^{-2}$) have concentrations that are nearly systematically lower than those from presumably accumulating surfaces.

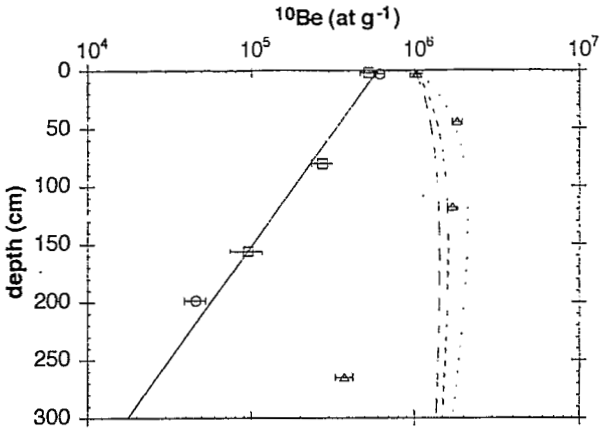


Fig. 4. Comparison of theoretical and measured distributions of $^{10}$Be as a function of subsurface depth in regions undergoing erosion and burial. On eroding surfaces, $^{10}$Be concentrations should decrease with depth with an exponential attenuation length of 170 g cm$^{-2}$ (continuous line). Measured $^{10}$Be concentrations in a quartz vein from the midland surface at Site BEF (○) show such behaviour. A family of curves is shown for depth distributions of $^{10}$Be in accumulating soils with burial rates of 2 (short dashes), 4 (medium dashes) and 6 (long dashes) m Myr$^{-1}$, and an initial surface concentrations of $\sim 10^6$ at g$^{-1}$. Measured $^{10}$Be in cobbles (Δ) in a lateritic soil at Site BSF profile show clear evidence of burial and, assuming that $^{10}$Be in the surface sample represents samples at initiation of their burial, are consistent with a burial rate of $\sim 3$ m Myr$^{-1}$. Samples from the paleochannel within the lowland surface at Mormossol (□, plotted as a function of depth below the surficial sandy–clayey layer) fall on an exponential decay line. This indicates that they have had the same relative positions for their entire exposure history.

burial and erosion. Thise is illustrated by the theoretical curves in Fig. 4. For eroding surfaces, Eq. 1 predicts exponential decreases with subsurface depth, which is is a direct consequence of lower production rates at depth due to the attenuation of cosmic ray neutrons. The erosion rate determines the surface concentration but has no influence on the slope (see Eqs. 1 and 2). The depth dependence of production rates influences material undergoing burial as well, and results in cosmogenic nuclide distributions in soil profiles in regions of accumulation which are very different from those in regions undergoing erosion. In a rock undergoing burial, the concentration increases with time until the rate of radioactive decay becomes greater than that of production. Calculations based on Eq. 3 show that subsurface maxima can be expected for the case of burial.

When overlain on Fig. 4, the data from Site BSF show clear evidence of burial, strongly contrasting with the exponential decrease in $^{10}$Be observed for the eroding vein quartz. The two samples at depth in the lateritic crust (BSF1-Q2 and BSF1-Q3) have $^{10}$Be concentrations that are 1.5 × to 2 × higher than those at the surface. Assuming that the sample from the outcropping vein (BSF1-Q1) represents the average source rock, the $^{10}$Be distributions in these samples are consistent with a burial rate of approximately 3 m Myr$^{-1}$. However, the sample (BSF1-Qr) taken from within the vein at the $\sim 2$ m depth does not at first appear to be consistent with either scenario. It has a concentration that is approximately 30 × higher than would be expected from a simple exponential decrease from the surface concentration, but considerably lower than that implied by the range of burial rates suggested by the other samples.

It is difficult to develop a quantitative history of the development of a lateritic profile with a small preliminary database. Nevertheless, these results are consistent with a model that assumes that the local topography was initially analogous to that observed presently at Site BEF and that the lower surface was then gradually buried. In this scenario, the west side of the quartz vein would have been a lower elevation surface undergoing accumulation and separated from an upper surface by an escarpment defined by the quartz vein. Sample BSF1-Qr would have been approximately 30 cm into this vertical face and would have undergone cosmic ray bombardment from the side. The angular distribution of cosmic ray particles has been approximated by a $\sin^{2.3}\theta$ dependence on the angle relative to the horizontal [44,45]. A rock exposed on a vertical cliff thus will have a production rate 50% lower than that of a horizontal surface at the same location. As material (including samples BSF1-Q2 and BSF1-Q3) accumulated on the lower plain, the cliff would have been buried and the production rate for sample BSF1-Qr would have decreased. Assuming that the vertical face was exposed for sufficient time to reach a steady-state concentration

(50% of that observed for BSF1-Q1 at the present outcropping vein surface), that the sample was at a horizontal depth of 30 cm from the vertical face, and that it was then buried at a rate of 3 m $Myr^{-1}$ (as implied by BSF1-Q2 and BSF1-Q3) a model of $^{10}Be$ accumulation yields a concentration of $\sim 400 \cdot 10^3$ at $g^{-1}$, consistent with the measured value of BSF1-Qr.

*Rapid deposition followed by accumulation*

At the third site (Mormosol, Fig. 2c) the texture of the soils within the profiles indicates that accumulation occurred in two distinct episodes, a period of high-energy rapid deposition (demonstrated by heterogeneity in soil texture) within a confined paleochannel followed by a period of slow gradual deposition (indicated by fine, well-sorted soil) across the fan surface. The samples, which come from three depths in the paleochannel, show an exponential decrease in $^{10}Be$ with depth (overlay on Fig. 4). The attenuation length calculated for this profile ($\sim 185$ g $cm^{-2}$ $yr^{-1}$) is a reasonable value for attenuation of cosmic ray neutrons at low geomagnetic latitude [23,24]. This implies that virtually all the $^{10}Be$ found in these samples was produced while they had the same relative positions, and requires either that the samples have always been in place or that they were exhumed from depth and rapidly deposited into their present relative positions. As noted above, field evidence suggests rapid deposition.

It is possible to constrain the timing of this deposition event using the $^{10}Be$ concentration of the sample at the interface between the soil layers. However, the calculated age is strongly dependent on the assumed deposition history of the surface layer. An exposure age of $\sim 2$ Myr can be calculated under the assumption that (contrary to field evidence based on grain size and soil texture) deposition of the upper layer occurred rapidly soon after that of the lower layer. A more realistic model (see Eq. 3) assumes constant slow burial after the initial rapid deposition of the lower layer, consistent with the observed soil textures, and yields an age of $\sim 300$ kyr and a mean burial rate of $\sim 5$ m $Myr^{-1}$, comparable with the rate of burial calculated for Site BSF. The assumptions that the overlying soil was deposited recently and rapidly and that the lower surface had suffered no erosional loss place a lower limit of $\sim 100$ kyr on the deposition age.

The second hypothesis is the most consistent with the granulometry of the lower (colluvial-like) and surficial (alluvial-like) layers and with the morphology of gold grains [46]. A 300 kyr age could correspond to the formation of the lowland lateritic system; this would have been coeval with the chemical and physical degradation (potentially associated with successive episodes of humid and dry climate) of the midland iron crust. The mean burial rate of $\sim 5$ m $Myr^{-1}$ would then represent the rate of subsequent (subrecent to present-day) erosional surface washing of the midland iron crust relict.

### 5.3. Use of the ratio $^{26}Al:^{10}Be$ in examining exposure / burial histories

The use of a pair of cosmogenic nuclides with different halflives can provide further information regarding exposure histories. Because of the shorter halflife of $^{26}Al$ the value of $^{26}Al:^{10}Be$ in a surficial rock decreases with exposure time, from the production ratio of $6.04 \pm 0.44$ to a steady-state ratio as low as 2.8 depending on the erosion rate [21]. Upon burial at sufficient depth for production to become negligible, $^{26}Al:^{10}Be$ decreases with an effective halflife of 1.3 Myr. Therefore, the position of a sample in $^{10}Be$–$^{26}Al:^{10}Be$ space may be used to differentiate between simple and complex exposure scenarios. Time-dependent trajectories associated with a range of erosion rates (from vanishingly small to infinitely large) define a region of simple surface exposure [see 21]. If samples fall below and to the left of this region, the indication is that they have had significant periods of shielding from cosmic rays. Conversely, samples falling to the right of the simple exposure zone have, in the past, been subject to higher production rates than those associated with their current positions. For samples collected at depth in a soil profile this suggests prior exposure at (or nearer to) the surface.

*Surface samples*

Measured values of $^{26}Al:^{10}Be$ from surface samples are generally consistent with surface ex-

posure and slow erosion rates (Table 1). However, one sample (BEF1-1SS) has a ratio significantly lower than would be expected for simple exposure at the surface. This value is lower than those of other samples from the same site, notably that of BEF1-1 which was collected from exactly the same location. Sample BEF1-1SS differs from the other samples from this site, being altered and friable rather than massive vein quartz. The fact that it is heavily altered is consistent with the notion that it has had a complex exposure history.

*Samples at depth in a profile*

Theoretical curves for the evolution of $^{26}Al:^{10}Be$ ratios and $^{10}Be$ concentrations were calculated for the present depths of the samples from Site BSF (Fig. 5). The rate of increase in $^{10}Be$ concentration is dependent on the production rate—and thus on the depth of a sample within a soil profile. The measured values of $^{26}Al:^{10}Be$ and $^{10}Be$ fall to the right of the curves calculated for their respective depths. This suggests that these samples have had complex histories involving prior surface exposure, consistent with the theory that they were mechanically transported by colluvial-like processes from nearby quartz veins. It should be noted that the model curves were calculated assuming no erosional loss; inclusion of erosion compresses the curves and moves them down and to the left, increasing their distances from the measured values. On the other hand, corrections for nucleogenic $^{26}Al$ would decrease these distances. However, as noted in the preceding section, this component is likely to be small ($< 400 \cdot 10^3$ at $g^{-1}$) and would not affect our conclusions. In spite of the relatively large propagated analytical uncertainties of the ratios, the coherence of the data and the fact that one sample (BSF1-Q3) is significantly different ($> 2\sigma$) from the production curve for its present depth provide further evidence for surface exposure in the past.

## 6. Summary

A series of stepped lateritic surfaces has been defined on a regional basis in West Africa. An

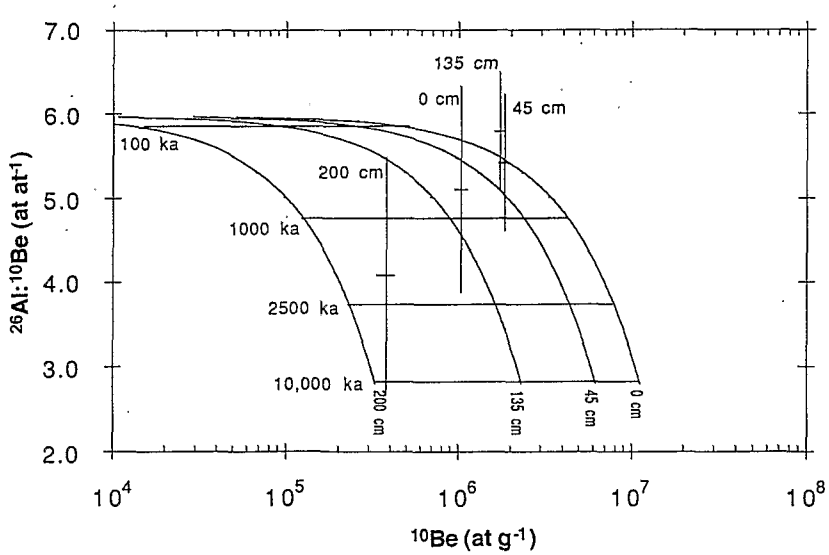


Fig. 5. $^{10}Be$–$^{26}Al:^{10}Be$ curves for the depths at Site BSF. The four growth trajectories correspond to the production rates associated with the present depths of the four samples, and are contoured for exposure time. Samples falling to the right of the trajectory associated with their present depths were subject to higher cosmic ray fluxes at some time during the past, indicating exposure closer to or at the surface.

understanding of the history of the development of these surfaces can be used to define periods with climatic conditions favourable for their formation and subsequent abandonment. The Eocene bauxite consists mainly of gibbsite, which is thermodynamically stable under humid tropical/subtropical conditions with over ~1700 mm of mean annual rainfall. It has been suggested that at the end of the Eocene a change of climate to drier tropical [47,48] induced chemical/physical degradation of the bauxitic surface and initiated the formation of iron crust systems. The highland, midland and lowland laterites—presumably formed successively since the Miocene—are believed to have developed under humid tropical climates with contrasting seasons and stabilized under drier conditions.

A preliminary study of distributions of $^{10}Be$ and $^{26}Al$ in iron crust lateritic surfaces in northern Burkina Faso has demonstrated the utility of *in-situ*-produced cosmogenic nuclides in discerning histories of exposure and erosion. More specifically, we have:

(1) calculated denudation rates of 3–8 m $Myr^{-1}$ for quartz veins outcropping in the midland lateritic system (comparable to values calculated for the Yilgarn Block Tertiary laterites in Western Australia, which are similarly stabilized by the present-day dry climate) and estimated burial rates of ~5 m $Ma^{-1}$ for lateritic soil profiles;

(2) shown that, consistent with theory, cobbles from actively accumulating surfaces have higher $^{10}Be$ concentrations than outcropping quartz veins in their source regions;

(3) demonstrated that soil profile cosmogenic nuclide distributions can be used for quantitatively distinguishing material with prior surface exposure (implying allochthonous formation) from material in place for long periods (implying autochthonous formation);

(4) estimated that an erosional/depositional event—potentially associated with the formation of the lowland system and hence with the last period of humid tropical conditions before initiation of drier climates leading to present-day subsahelian conditions—occurred approximately 300 kyr BP.

## Acknowledgements

Discussion with Bruno Boulangé, Georges Grandin and Ed Brook and reviews by James Arnold, George Brimhall and Robert Stallard greatly improved the quality of this work. We thank Jacques Lestringuez and Dominique Deboffle for their continuing expertise in AMS measurements and Professor Bernard Platevoët for providing access to sample preparation facilities. This work was supported by INSU through the DBT Programme (DBTF 1/01). Tandetron operation is supported by the CNRS, CEA and $IN_2P_3$. Logistic support was from the ORSTOM Centre, Ouagadougou, Burkina Faso.

## References

[1] R.F. Stallard, Weathering and erosion in the humid tropics, in: Physical and Chemical Weathering in Geochemical Cycles, A. Lerman and M. Meybeck, eds., pp. 225–246, Kluwer, Dordrecht, 1988.

[2] F. Colin, G. Brimhall, D. Nahon, C.J. Lewis, A. Baronnet and K. Danti, Equatorial rainforest lateritic soils: A geomembrane filter, Geology 20, 523–526, 1992.

[3] Y. Tardy, Pétrologie des Latérites et des Sols Tropicaux, 461 pp., Masson, Paris, 1993.

[4] G.H. Brimhall, C.J. Lewis, C. Ford, J. Bratt, G. Taylor and O. Warin, Quantitative geochemical approach to pedogenesis: importance of parent material, regolith reduction, volumetric expansion and eolian influx in lateritization, Geoderma 51, 51–91, 1991.

[5] D. Nahon, Introduction to the Petrology of Soils and Chemical Weathering, 313 pp., Wiley, New York, 1991.

[6] D. Nahon, Evolution of iron crusts in tropical landscapes, in: Rates of Chemical Weathering of Rocks and Minerals, S.M. Colman and D.P. Dethier, eds., pp. 169–191, Academic Press, Orlando, 1986.

[7] J.P. Ambrosi, Modélisation thermodynamique de l'altération latéritique dans le système $Fe_2O_3$–$SiO_2$–$H_2O$, Ph.D. Thesis, Univ. Aix-Marseille III, 1990.

[8] P. Michel, Les bassins des fleuves Sénégal et Gambie, Mém. ORSTOM 3, 752, 1970.

[9] J. Delvigne and G. Grandin, Etude des cycles morphogénétiques et tentative de chronologie paléoclimatique dans la région de Tormodi, en Côte d'Ivoire, C.R. Acad. Sci. Paris 15, 1372–1375, 1969.

[10] B. Boulangé, J. Delvigne and V. Eschenbrenner, Descriptions morphoscopiques, géochimiques et minéralogiques des faciès cuirassés des principaux niveaux géomorphologiques de Côte d'Ivoire, Cah. ORSTOM, Sér. Géol. 1, 59–81, 1973.

[11] D. Nahon and J.R. Lappartient, Time factor and geochemistry in iron crust genesis, Catena 4, 249–254, 1977.
[12] G. Bocquier, C. Bernard and A.P. Boulad, Utilisation des isotopes stables et radioactifs pour la détermination des conditions anciennes et des vitesses de l'altération, Bull. Assoc. Fr. Etud. Sols 2–3, 137–147, 1976.
[13] M.M. Bernard, G. Bocquier and M. Javoy, Détermination des rapports isotopiques $^{18}O/^{16}O$ de la gibbsite et de la boehmite dans différentes bauxites, C.R. Acad. Sci. Paris 282D, 1089–1092, 1979.
[14] M.I. Bird and A.R. Chivas, Oxygen isotope dating of the Australian regolith, Nature 331, 513–516, 1988.
[15] S. Giral, D. Nahon, J.P. Girard and S.M. Savin, Variation in $^{18}O/^{16}O$ ratios of kaolinites within a lateritic profile: their significance for laterite genesis and isotope paleoclimatology, Geol. Soc. Am. Abstr. Programs 24, A70, 1992.
[16] P.M. Vasconselos, T. Becker, P.R. Renne and G.H. Brimhall, Age and duration of weathering by $^{40}K$:$^{40}Ar$ analysis of potassium–manganese oxides, Science 258, 451–455, 1992.
[17] G. Bárdossy, Karst Bauxite, 441 pp., Elsevier, Amsterdam, 1982.
[18] R.A. Berner, A.C. Lasaga and R.M. Garrels, The carbonate–silicate geochemical cycle and its effect on atmospheric carbon dioxide over the past 100 million years, Am. J. Sci. 283, 641–643, 1983.
[19] L.A. Frakes, Climates Throughout Geologic Times, 310 pp., Elsevier, Amsterdam, 1976.
[20] E.T. Brown, J.M. Edmond, G.M. Raisbeck, F. Yiou, M.D. Kurz and E.J. Brook, Examination of surface exposure ages of moraines in Arena Valley, Antarctica using in situ produced $^{10}Be$ and $^{26}Al$, Geochim. Cosmochim. Acta 55, 2269–2283, 1991.
[21] D. Lal, Cosmic ray labeling of erosion surfaces: in situ nuclide production rates and erosion models, Earth Planet. Sci. Lett. 104, 424–439, 1991.
[22] E.T. Brown, E.J. Brook, G.M. Raisbeck, F. Yiou and M.D. Kurz, Effective attenuation lengths of cosmic rays producing $^{10}Be$ and $^{26}Al$ in quartz: Implications for exposure age dating, Geophys. Res. Lett. 19, 369–372, 1992.
[23] M.D. Kurz, In situ production of terrestrial cosmogenic helium and some applications to geochronology, Geochim. Cosmochim. Acta 50, 2855–2862, 1986.
[24] P. Sarda, T. Staudacher, C. Allègre and A. Lecomte, Cosmogenic neon and helium at Réunion: measurement of erosion rate, Earth Planet. Sci. Lett. 119, 405–417, 1993.
[25] D. Lal, K. Nishiizumi and J. Arnold, In situ cosmogenic $^{3}H$, $^{14}C$ and $^{10}Be$ for determining the net accumulation and ablation rates of ice sheets, J. Geophys. Res. 92, 4947–4952, 1987.
[26] J. Klein, R. Giegengack, R. Middleton, J.R. Underwood, Jr. and R.A. Weeks, Revealing histories of exposure using in situ-produced $^{26}Al$ and $^{10}Be$ in Libyan Desert Glass, Radiocarbon 28, 547–555, 1986.
[27] B. Boulangé, Les formations bauxitiques latéritiques de Côte d'Ivoire, Mém. ORSTOM 175, 341, 1984.
[28] G. Grandin, Aplanissements cuirassés et enrichissement des gisements de manganèse dans quelques régions d'Afrique de l'Ouest, Mém. ORSTOM 82, 1–275, 1973.
[29] J.P. Milesi, Les minéralisations aurifères de l'Afrique de l'Ouest. Leurs relations avec l'évolution lithostructurale au Protérozoïque inférieur, Chron. MInes Rech. Miniere 497, 3–98, 1989.
[30] S. Nikiema, Le Birrimien du nord du Burkina Faso, Ph.D. Thesis, Univ. Cheik Anta Diop, Dakar, 1992.
[31] D.L. Bourlès, Etude de la géochimie de l'isotope cosmogénique $^{10}Be$ et de son isotope stable $^{9}Be$ en milieu océanique: Application à la datation des sédiments marins, Ph.D. Thesis, Univ. Paris XI, 1988.
[32] G.M. Raisbeck, F. Yiou, D. Bourlès, J. Lestringuez and D. Deboffle, Measurements of $^{10}Be$ and $^{26}Al$ with a Tandetron AMS facility, Nucl. Instrum. Methods B29, 22–26, 1987.
[33] E.J. Brook and M.D. Kurz, Surface-exposure chronology using in situ cosmogenic $^{3}He$ in Antarctic quartz sandstone boulders, Quat. Res. 39, 1–10, 1993.
[34] K. Nishiizumi, E.L. Winterer, C.P. Kohl, J. Klein, R. Middleton, D. Lal and J.R. Arnold, Cosmic ray production rates of $^{10}Be$ and $^{26}Al$ in quartz from glacially polished rocks, J. Geophys. Res. 94, 17907–17915, 1989.
[35] E.J. Brook et al., Cosmogenic nuclide exposure ages and glacial history of late Quaternary Ross Sea Drift in McMurdo Sound, Antarctica, Boreas, in prep., 1994.
[36] P. Sharma and R. Middleton, Radiogenic production of $^{10}Be$ and $^{26}Al$ in uranium and thorium ores: Implications for studying terrestrial samples containing low levels of $^{10}Be$ and $^{26}Al$, Geochim. Cosmochim. Acta 53, 709–716, 1989.
[37] J.Y. Gac, Géochimie du bassin du Lac Tchad. Bilan de l'altération, de l'érosion et de la sédimentation, Trav. Doc. ORSTOM 123, 1–251, 1980.
[38] E.T. Brown, R.F. Stallard, G.M. Raisbeck and F. Yiou, Determination of the denudation rate of Mount Roraima, Venezuela using cosmogenic $^{10}Be$ and $^{26}Al$, EOS 73, 170, 1992.
[39] L.C. King, A geological comparison between Eastern Brazil and Africa (Central and Southern), Q.J. Geol. Soc. London 112, 445–474, 1956.
[40] R.W. Fairbridge and C.W. Finkl, Geomorphic analysis of the rift cratonic margins of Western Australia, Z. Geomorph. 22, 369–389, 1978.
[41] R.W. Fairbridge and C.W. Finkl, Cratonic erosion unconformities and peneplains, J. Geol. 88, 69–86, 1980.
[42] E.M. Shoemaker, C.S. Shoemaker, K. Nishiizumi, C.P. Kohl, J.R. Arnold, J. Klein, D. Fink, R. Middleton, P.W. Kubik and P. Sharma, Ages of Australian meteorite craters—a preliminary report, Meteoritics 25, 409, 1990.
[43] K. Nishiizumi, C.P. Kohl, J.R. Arnold, M.W. Caffee, R.C. Finkel, J. Southon, E.M. Shoemaker and C.S. Shoe-

maker, Exposure histories of desert sands using in situ produced cosmogenic nuclides, EOS 73, 185, 1992.
[44] M. Conversi and P. Rothwell, Angular distributions in cosmic ray stars at 3500 m, Nuovo Cimento 12, 191–211, 1954.
[45] D. Lal, Investigations of nuclear interactions produced by cosmic rays, Ph.D. Thesis, Tata Inst. Fundam. Res., Bombay, 1958.
[46] F. Colin, Z. Sanfo, E.T. Brown and D.L. Bourlès, Gold: a physical and chemical tracer in laterites, in prep., 1994.
[47] J.T. Parrish, A.M. Zirgler and C.R. Scotese, Rainfall patterns and the distribution of coals and evaporites of the Mesozoic and Cenozoic, Palaeogr., Palaeoclimatol., Palaeoecol. 40, 67–101, 1982.
[48] B. Kobilsec, Géochimie et pétrographie des bauxites latéritiques d'Amazonie Brésilienne. Comparaison avec l'Afrique, l'Inde et l'Australie, Ph.D. Thesis, Univ. Louis Pasteur, Strasbourg, 1990.